*Rev. Roum. Sci. Techn.– Électrotechn. et Énerg.*
Vol. **71**, *2*, pp. 253–258, Bucarest, 2026

# CONTACT RESISTANCE OF COPPER CONTACT WITH ZrCu THIN LAYER DURING ACCELERATED AGING

GIDEON GWANZUWANG DANKAT[1], GEORGE CRISTIAN LAZAROIU[1], LAURENTIU MARIUS DUMITRAN[1], ANCA CONSTANTINA PARAU[2], ALINA VLADESCU (DRAGOMIR) [2]

**Keywords: Electrical contact; Accelerated aging; Contact resistance; Zirconium Copper (ZrCu) alloy spots.**

**Reliability of electrical connectors is increasingly critical in modern automotive systems, particularly as the industry transitions toward fully electric vehicles with dense sensor networks and expanded data processing needs. Failures in connector interfaces can lead to severe system malfunction, equipment damage, or safety hazards. Among the various environmental and mechanical stressors that affect connector performance, electrical contact degradation, often evidenced by increased contact resistance, remains a primary concern. This study investigates the mechanisms and progression of contact degradation through controlled thermal aging of fabricated samples. ZrCu alloy coatings were deposited onto copper-clad laminates using cathodic arc technology to create representative contact interfaces. The evolution of contact resistance was monitored under low-current, low-voltage conditions to capture early-stage degradation effects. Results show a clear increase in resistance with aging, confirming the sensitivity of contact performance to factors such as oxidation, temperature exposure, and surface contamination. Additionally, the applied contact load was found to influence the effective contact area, thereby affecting overall resistance behavior.**

## 1. INTRODUCTION

Electrical contacts play a central role in ensuring that power and signals are transferred reliably in many electronic and automotive systems. One of the key indicators of connector performance is contact resistance, which reflects how well two metal surfaces conduct electricity when pressed together [1]. Good performance depends on having a clean and sufficiently large real contact area. Quantitatively, the real contact area can be expressed as

$$S_{real} = S_n(1-\alpha)(1-\gamma), \quad (1)$$

where $S_n$ is the nominal contact area, α is the void ratio, and $1-\gamma$ is the conductive volume ratio. Since the contact resistance is inversely proportional to the real contact area,

$$R_C = \rho h_0 / S_{real}, \quad (2)$$

where ρ is the resistivity of the conductors and $h_0$ the height. A larger real contact area results in lower contact resistance [2]. As vehicles become more electrified and include more electronic features, the demand for dependable connectors continues to grow.

Electric and hybrid vehicles now rely on large networks of sensors and control modules to support important functions such as adaptive cruise control, emergency braking, lane keeping assistance, keyless entry, and airbag deployment [3]. These systems require many reliable electrical interfaces, and industry reports predict continued growth in the global connector market as safety and connectivity features become standard [3,4]. Because connectors operate in harsh environments, high temperatures, vibration, humidity, and corrosive atmospheres, they are especially vulnerable to long-term degradation. Saliha et al. showed that rain-induced humidity, polymer degradation, material corrosion, and temperature fluctuations contributed to a decrease in insulation resistance in photovoltaic systems, leading to inverter disconnection under adverse weather conditions [5]. Increased contact resistance is one of the most common signs of connector failure, and is often responsible for more than half of electrical problems in vehicles. Studies have shown that automotive connectors may face temperatures exceeding 85–150 °C during normal operation, which speeds up oxidation and mechanical wear [6]. Although automotive connectors can experience peak temperatures of 85–150°C depending on installation location, an aging temperature of 50°C was selected in this study as a controlled mild-aging condition rather than peak under-hood extremes.

Several studies have investigated how and why electrical contacts degrade over time. Some work has focused on developing models to estimate contact resistance on rough metallic surfaces, showing that increasing the true contact area can help limit the temperature rise during operation. For example, increasing the contact radius from 2 – 6 mm (*i.e.*, increasing the real contact area) reduces the contact temperature from 76 °C to 48 °C for AgCdO contact surface models with surface roughness characterized by arithmetic mean roughness values (Ra = 0.166 – 0.169 μm) and root mean square (RMS) roughness (σ = 0.208 – 0.212 μm) for AgCdO contact surfaces, with asperity heights typically following a Gaussian distribution [7]. Other research examining tin-plated connectors under fretting motion for an applied load of 3 N and a current of 10 mA found that areas without oxide films exhibit low resistance (15 mΩ), while regions with thicker oxide layers (5 μm thickness) display significantly higher resistance, typically exceeding 50 mΩ after 60 fretting cycles [8]. Additional studies have explored how the geometry of the contact interface influences constriction resistance, using controlled, microscale test structures to simulate real contact conditions [9]. One reason electrical contacts degrade is that the real conducting area between the two metal surfaces is much smaller than it appears. Instead of touching across the entire visible region, the surfaces meet only at several microscopic high points known as asperities (Fig. 1).

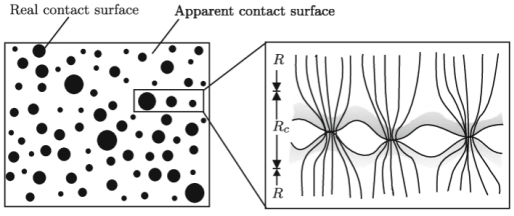


Fig. 1 – A general illustration of an electrical contact interface [10].

These small contact spots cause the electrical current to narrow, or "constrict," as it passes from one surface to the other, thereby increasing overall resistance [11,12]. Contact force also plays a major role: increasing contact loads from approximately 0.2 to 2.5 N for automotive sensor connectors is shown experimentally to significantly increase the true

[1] Faculty of Electrical Engineering, National University of Science and Technology Politehnica Bucharest, Bucharest, Romania.
[2] National Institute of Research and Development for Optoelectronics – INOE 2000, 409 Atomistilor St. Magurele, RO77125, Romania.
E-mails: gideon.dankat1004@upb.ro, gdankat@elmat.pub.ro (correspondence), dumitran@elmat.pub.ro, Cristian.lazaroiu@upb.ro, alinava@inoe.ro, anca.parau@inoe.ro

DOI: 10.59277/RRST-EE.2026.2.14

contact area, leading to a sharp reduction in contact resistance (mΩ), while larger loads ~ 2.5 – 7 N exhibit a nearly constant contact resistance [13].

Connector performance does not just affect the safety and reliability of electric vehicles, but it can also affect the electric vehicle charging stations by increased conduction losses in semiconductor devices due to temperature or degradation, which leads to power loss [14]. Therefore, understanding how contact resistance changes as materials age remains an important research focus. In this study, ZrCu-coated copper samples were subjected to accelerated thermal aging to examine how the contact resistance evolves over time. Measurements were taken under low-current and low-voltage conditions to capture early changes in degradation. The results show that resistance grows steadily as thermal exposure increases, while higher contact loads improve the effective contact interface.

Results for 1 µm and 10 µm ZrCu contact spots were previously reported in [15,16] and are included in this report for comparison with the new 13 µm ZrCu contact spots measurements.

## 2. EXPERIMENTAL SAMPLES AND PROCEDURES

### 2.1. SAMPLE PREPARATION

To create experimental samples representing multi-spot electrical contacts, copper-clad laminate (CCL) sheets were prepared as the base material. Both the upper and lower electrodes were cut into rectangular pieces measuring 55 mm × 17 mm. For the lower electrode, a section of a printed circuit board (PCB) prototype was trimmed into a 17 mm × 17 mm square and contained 36 holes that served as a masking pattern for the ZrCu coating process (Fig. 2). Before coating, all substrates were ultrasonically cleaned in isopropanol for 10 minutes (Fig. 3). A ZrCu alloy film ranging from 1 to 13 µm thick was then applied using the cathodic arc deposition unit manufactured by the Kharkov Institute of Physics and Technology (KIPT) in the 1970s (Fig. 4).

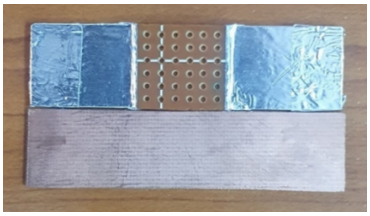

a)

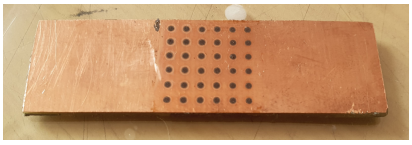

b)

Fig. 2 – Contact samples: a) before ZrCu coatings deposition; b) after ZrCu coatings deposition [15].

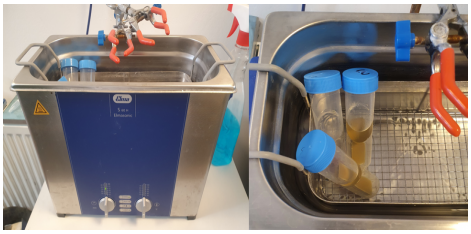

Fig. 3 – Samples ultrasonically cleaned in isopropanol.

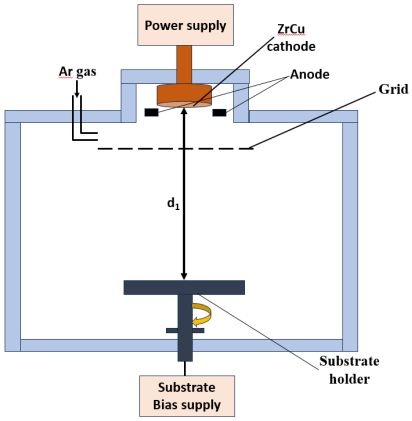


Fig. 4 – schematic of the deposition chamber [17].

The deposition system operated with a single ZrCu alloy cathode (50 at. % Zr and 50 at. % Cu, 99.9% purity) having a diameter of 115.5 mm and a thickness of 25 mm, supplied by Cathay Advanced Materials Limited (China) and the samples were placed at ($d_1$ = 500 mm) from the cathode. The samples were placed on a rotating substrate holder during coating to ensure a uniform film composition, while the rotating speed was maintained at approximately 3 rpm during deposition. The ZrCu films on Si wafers and Cu substrates were deposited simultaneously under identical conditions in a single run. Si wafers were used for XRD and EDS to avoid interference from Cu substrate signals and enable clearer identification of coating-related peaks. The chamber was maintained at a base pressure of $10^{-3}$ Pa. Before the coating process, the surfaces were cleaned by Ar sputter etching at $10^{-1}$ Pa for 15 min under a −950 V bias. Deposition was then carried out at an Ar pressure of $2\times10^{-2}$ Pa with a gas flow of 20 sccm. The arc current was set to 60 A, and a −100 V bias was applied to the substrates. The deposition temperature reached approximately 340 °C. By adjusting the coating duration from 20 to 100 min, films with thicknesses ranging from 1 to 13 µm were produced. The distribution and geometry of the resulting contact spots on the CCL surface were controlled by the PCB mask used during deposition.

### 2.2 EXPERIMENTAL METHODS

The elemental composition of the coatings was analyzed using a scanning electron microscope (SEM) performed at an accelerating voltage of 5 kV, equipped with an energy dispersive X-ray spectroscopy (EDS detector: TableTop 3030PLUS with Quantax70, Bruker). Surface morphology was evaluated by SEM, while X-ray diffraction (XRD) analysis to determine the phase composition and texture was done by grazing XRD using a Rigaku SmartLab diffractometer equipped with CuKα radiation (λ = 1.5406 Å). The measurements were performed in θ-2θ geometry over the 2θ range of 10-100°, with a step size of 0.02° and an incidence angle of 3°. Coating roughness and thickness were measured with a Dektak 150 profilometer fitted with a 2.5 µm stylus diameter. Roughness measurements were carried out over a 100 µm scan length at a stylus force of 5 mg in three randomly selected regions of each sample. EDS analysis was carried out on coatings deposited on Si wafers with dimensions 15 ×15 $mm^2$ to allow clear identification of each constituent element. The ZrCu films grown on Si wafers and Cu substrates were deposited under identical conditions, with all substrates placed on the same holder and processed simultaneously in a single deposition run. The use of Si wafers was intended for XRD and

EDS characterizations to prevent peak overlap arising from the presence of Cu in both the coating and the Cu substrates, which would otherwise hinder the clear identification of diffraction/EDS peaks associated with the coating.

Contact resistance measurements were performed using the four-wire (Kelvin) resistance technique (Fig. 5a). The experimental setup included a contact measurement assembly, calibrated loading weights, and a Keithley 2700 digital multimeter. The multimeter supports current ranges from 10 nA to 3 A (DCI) and 1 μA to 3 A RMS (AC), as well as voltage ranges of 0.1 μV to 1000 V (DC) and 0.1 μV to 750 V RMS (ACV). The applied current was limited to 10 mA, with a maximum open-circuit voltage of 20 mV in all experiments. The contact samples were arranged in a cross-shaped configuration and mounted onto the measurement assembly before testing. Contact resistance measurements were conducted using applied loads of 500 g, 700 g, 800 g, and 820 g [15,16]. The loading weights were positioned at different locations on the platform of the measurement assembly to account for minor variations in the deposited contact spots, which resulted in differences in effective contact area and measured contact resistance (Fig. 5b).

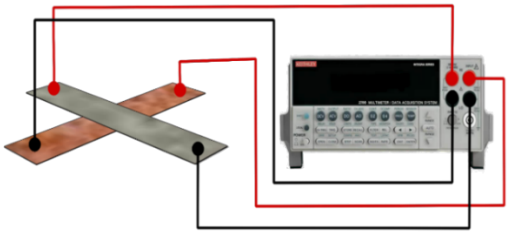

a)

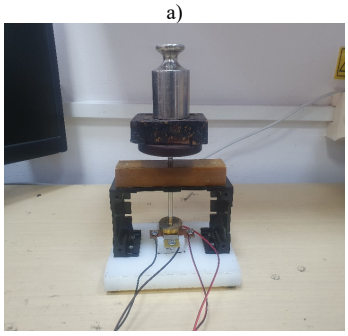

b)

Fig. 5 – Experimental method: a) Four-wire (Kelvin) resistance measurement; b) measurement assembly [15,16].

Fig. 6 – Contact samples aged in a forced air oven under a sodium chloride (NaCl) atmosphere [15,16].

Initial contact resistance values were recorded for all samples before accelerated aging. The samples were then subjected to accelerated aging in an air forced oven for 277 hours at a temperature $T = 50$ °C in the presence of a free-floating sodium chloride solution (Fig. 6). Following every aging interval, the samples were removed from the forced flow oven, then mounted on the measuring assembly, and contact resistance measurements were carried out at ambient temperature.

## 3. RESULTS

Figure 7 shows the resulting EDS spectrum (a) and elemental distribution maps (b). The maps indicate that all elements within the coating are uniformly distributed across the examined surface.

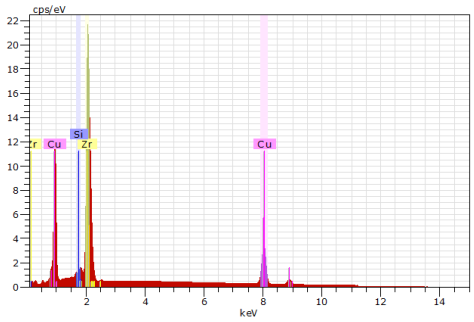


a)

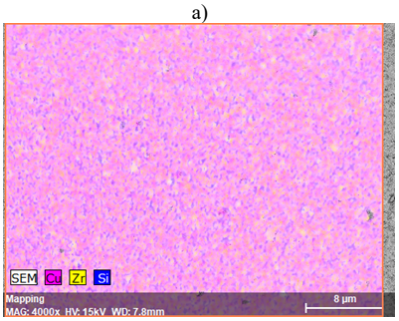


b)

Fig. 7 – EDS analysis: a) EDS spectrum; b) Distribution of all elements of coating.

XRD diffraction pattern of the coating deposited on Si wafer substrate, together with the pattern of the Si wafer itself, is presented in Fig. 8. The coating indicates an amorphous structure, which is characteristic of ZrCu metallic glass thin films [18,19]. Although the substrate temperature during deposition can reach ~350 °C due to intrinsic plasma heating, the amorphous structure of the Zr-Cu coatings is not primarily determined by temperature.

The formation of the amorphous phase is mainly attributed to the high glass-forming ability of the Zr-Cu system, which is strongly influenced by the significant atomic size mismatch between its constituent elements. The atomic radius of Cu (~0.128 nm) and Zr (~0.160 nm) results in a mismatch of approximately 25%, well above the ~12% threshold generally considered necessary to promote amorphization. This substantial size difference disrupts efficient atomic packing and inhibits long-range atomic ordering, thereby suppressing crystallization. In addition, the negative enthalpy of mixing and the instability of competing crystalline phases in the Zr-Cu system further favor the formation of a disordered structure. Consequently, under the non-equilibrium conditions of cathodic arc deposition, these factors collectively promote the formation of amorphous coatings, even at elevated substrate temperatures [20]. Figure 9 shows an example of the coating thickness measured in two different areas of the sample. Figure 10 shows the surface morphology of the coating. The surface appears uniform and free of major defects. A few microdroplets are visible, a common feature of coatings produced by cathodic arc deposition.

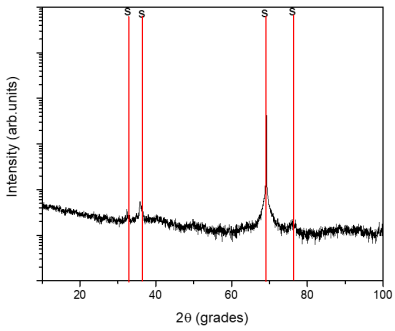


Fig. 8 – XRD diffraction patterns of the ZrCu coatings (s - Si peaks of substrate according to JCPDS card no. 026-1481).

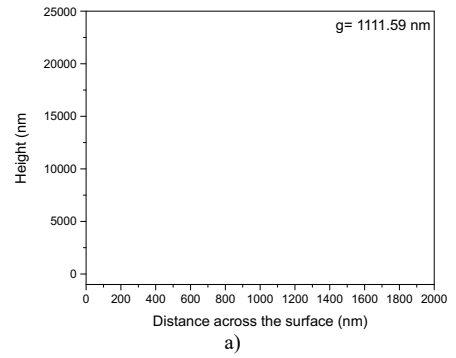


a)

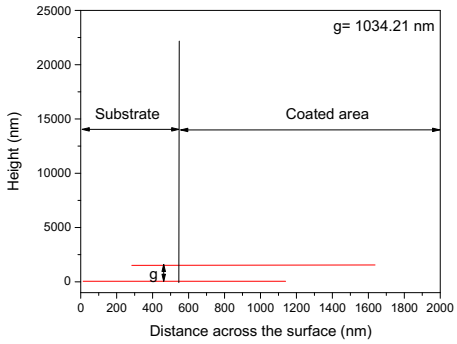


b)

Fig. 9 – Thickness of the coatings measured different areas of a sample (randomly selected): a) Area 1; b) Area 2 [15].

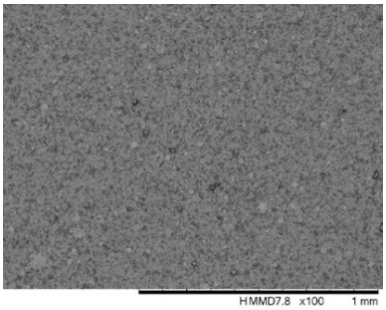


Fig. 10 – Morphology on the coating surface [15].

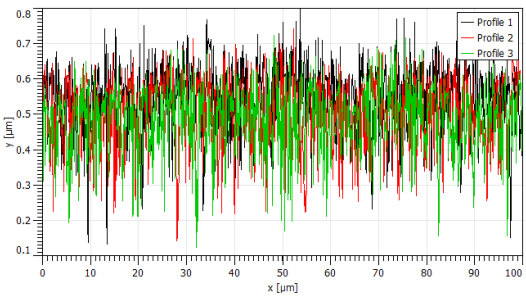


Fig. 11 – Roughness Profile of the surface.

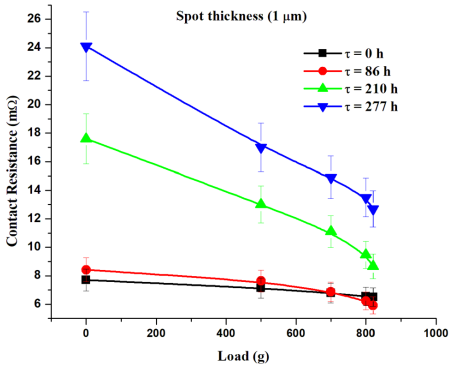


a)

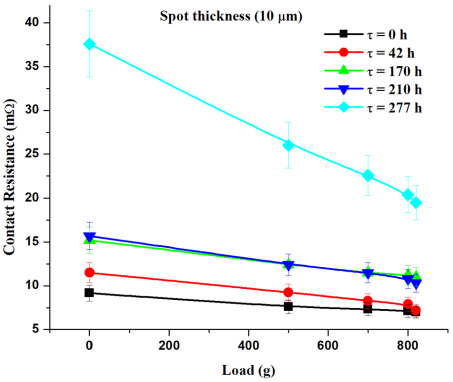


b)

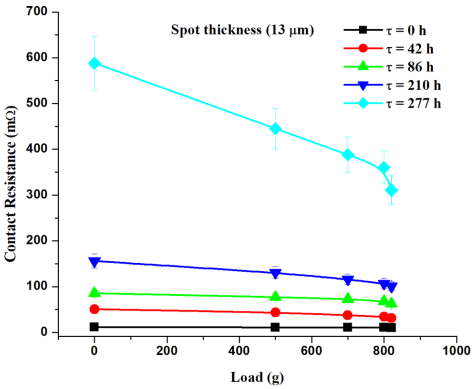


c).

Fig. 12 – Contact resistance variation with contact load for different aging time: (a) Contact spot thickness 1 µm [15]; (b) Contact spot thickness 10 µm [16]; (c) Contact spot thickness 13 µm.

Overall, the surface features are evenly distributed, and the coating exhibits fine, consistent grains across the entire area. The surface roughness in three randomly selected regions (Fig. 11) of each sample. The reported roughness values (roughness average (Ra): 0.071 µm and root mean square roughness (Rq): 0.092 µm) correspond to the average of these measurements. Figure 12 shows the variation in contact resistance with contact load for three contact samples with contact spot thicknesses of 1 µm, 10 µm, and 13 µm. The results are presented for different aging times and were obtained by averaging measurements taken at multiple applied force points on the measuring platform. The contact variation against contact load for a contact spot thickness of 1 µm is presented in Fig. 12a. The results show that as the contact load increases from 0 to 500 g, the contact resistance consistently decreases for all aging times. Specifically, the resistance drops from 7.7 mΩ to 6.7 mΩ at 0 h, from 8.4 mΩ to 6.8 mΩ at 86 h, from 17.6 mΩ to 11.1 mΩ at 210 h, and from 24.1 mΩ to 14.9 mΩ at 277 h when the load is further increased to 820 g, the contact resistance slightly decreases to 6.5 mΩ (0 h), 5.9 mΩ (86 h), 8.6 mΩ (210 h), and 12.7 mΩ (277 h),

respectively [15]. Presented in Fig. 12b is the contact variation against contact load for a contact spot thickness of 10 μm. According to the results, the contact resistance decreases from 9.2 mΩ to 7.3 mΩ at 0 h, from 15.7 mΩ to 11.5 mΩ at 86 h, from 24 mΩ to 11.9 mΩ at 210 h, and from 37.6 mΩ to 22.6 mΩ at 277 h when the contact load is raised from 0 to 500 g. At a contact load of 820 g, the contact resistance further drops to 7 mΩ (0 h), 10.3 mΩ (86 h), 10.5 mΩ (210 h), and 19.5 mΩ (277 h) [16]. For a contact spot thickness of 13 μm, the contact resistance variation against contact load is depicted in Fig. 12c. The results show that increasing the contact load from 0 to 500 g leads to a reduction in contact resistance at all aging times. In particular, the resistance decreases from 11.5 mΩ to 10.6 mΩ at 0 h, from 85.6 mΩ to 72.9 mΩ at 86 h, from 156 mΩ to 116 mΩ at 210 h, and from 588 mΩ to 388 mΩ at 277 h. When the contact load is further increased to 820 g, the contact resistance becomes 9.7 mΩ, 60.9 mΩ, 95.3 mΩ, and 285 mΩ for aging times of 0 h, 86 h, 210 h, and 277 h, respectively.

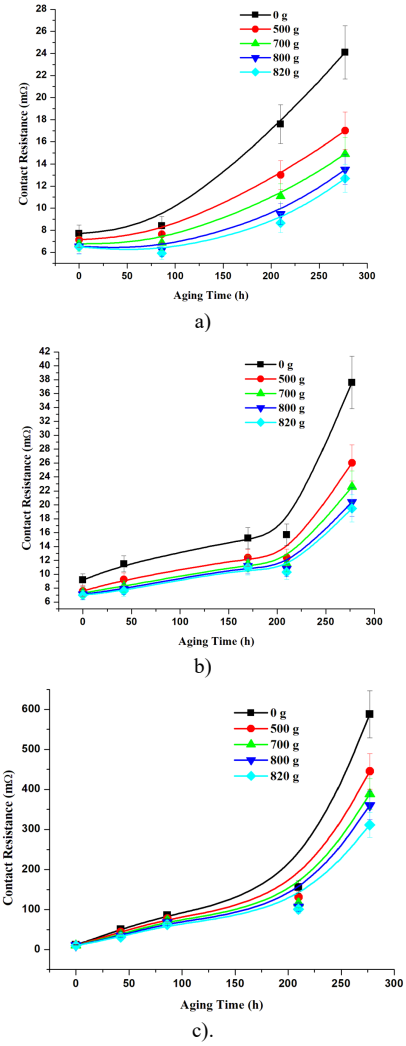


Fig. 13 – Contact resistance variation with aging time for different contact load: (a) Contact spot thickness 1 μm [15]; (b) Contact spot thickness 10 μm [16]; (c) Contact spot thickness 13 μm.

Figure 13 presents the contact resistance variation with aging time under applied loads from 0 g to 820 g for three contact samples with contact spot thicknesses of 1 μm (Fig. 13a), 10 μm (Fig. 13b), and 13 μm (Fig. 13c). The results presented as expected, clearly depict that contact resistance increased with aging time for all conditions; however, higher applied loads resulted in consistently lower resistance values. Differences among the loading conditions were minimal at early aging times but became more pronounced at longer aging durations, indicating that increased contact force mitigates the accelerated aging-induced rise in contact resistance.

The error bars in Figs. 12 and 13 show the standard deviation of repeated contact resistance measurements. Small error bars before aging indicate good repeatability. As thermal aging time increases, both the mean contact resistance and the error bars increase, especially at longer aging times, indicating greater variability in electrical contact behavior, likely due to increased surface and interfacial inhomogeneity.

## 4. DISCUSSION

As illustrated in Fig. 12, the results indicate that for all contact spot thicknesses (1 μm, 10 μm, and 13 μm), contact resistance decreases with increasing contact load; these characteristics can be attributed to the increase in real contact area under higher applied mechanical load, which reduces constriction resistance at the contact interface. The observed contact resistance to contact load relationship is consistent with reported findings in [21,22], with measured contact resistance values remaining in the milliohm range under low-level test conditions (10 mA, open circuit voltage < 20 mV), consistent with IEC-512-2-2a (test current ≤ 100 mA; open circuit voltage ≤ 20 mV).

As expected, a considerable increase in contact resistance is observed with increasing aging time across all spot thicknesses. At aging time (0 h), the contacts exhibit the lowest resistance values, whereas prolonged aging times (210 h) and (270 h) lead to a significant rise in resistance. This increase may be associated with surface degradation and aging-related interfacial changes, which can impede electrical conduction at the contact interface and increase the contact resistance.

The effect of contact spot thickness on contact resistance is also evident. For the experimentally contacted sample with the smallest thickness (1 μm), resistance values remain relatively low even after extended accelerated aging. However, contact with larger spot thicknesses (10 μm and 13 μm) shows substantially higher resistance, particularly at longer aging times. This trend highlights that thicker spots promote the formation of insulating surface layers, which limit the real contact area at the interface and lead to higher resistance. As reported in [8], this behavior is typical of aged electrical contacts, in which regions of the contact interface with high concentrations of contaminants exhibit increased resistance, whereas regions with little or no contamination exhibit lower resistance.

In Fig. 13, the experimental study for the fabricated contact samples with spot thicknesses (1 μm, 10 μm, and 13 μm) clearly shows the thermal effect on contact resistance by the rise in contact resistance as the aging time increases in all cases, indicating progressive degradation of the contact interface. This behavior is attributed to the accumulation of contaminants and the effects of environmental factors such as temperature, oxide formation, and humidity. Over time, the continuous increase in contact resistance leads to the deterioration of electrical contacts and can ultimately result in contact failure.

The contact resistance investigations carried out on contact samples, such as those in this study, using a four-point probe under low-level current conditions, are quite complex. Although all measurements were carefully controlled and monitored, it was not possible to ensure that electrical contact was made at the same point during repeated measurements. Overall, the contact resistance trends remain reliable and indicative of the contact resistance behavior in degraded electrical contacts. The

deposition of ZrCu alloy on the copper substrates was intended to slightly alter the electrical characteristics of the contacts, because reported electrical resistivity values of amorphous $Zr_{50}Cu_{50}$ alloy ($2–2.2\times10^{-6}$ Ωm) [23] are much higher than that of copper ($1.7–1.8\times10^{-8}$ Ωm) [24]. The electrical resistivity of $Zr_{50}Cu_{50}$ cathode used in the present study was not measured directly. However, considering that the cathode material is a metallic alloy, its electrical resistivity is expected to fall within the typical range reported for Zr-Cu systems. It is important to note that, in cathodic arc deposition, the process is mainly controlled by arc plasma characteristics and cathode spot behavior, and is not significantly influenced by the bulk resistivity of the cathode material. Nevertheless, direct resistivity measurements of the cathode would provide additional confirmation and will be considered in future work. These deposited ZrCu spots act as contact regions at the interface between two substrates in contact; however, electrical contact does not occur uniformly across the entire coated area but is instead established at localized points within these contact regions. As a result, the measured resistance reflects the contribution of these higher resistivity contact spots.

## 5. CONCLUSIONS

This study experimentally analyzed the electrical contact resistance of copper substrates coated with ZrCu alloy spots with different thicknesses (1 μm, 10 μm, and 13 μm), which were subjected to accelerated thermal aging. Contact resistance was measured using the four-point probe resistance measurement method and a Keithley 2700 multimeter. Although measurements were conducted at a relatively low current level (10 mA), the results effectively characterize the behavior of degraded electrical contacts. The findings demonstrate that thermal aging significantly influences the electrical performance of the investigated contact material.

## ACKNOWLEDGEMENT

This research was funded by a grant from the Ministry of Research, Innovation, and Digitalization, project number PNRR-C9-I8-760089/23.05.2023, code CF 31/14.11/2022.

The 4th and 5th authors acknowledge INOE research funded by the Romanian Ministry of Research, Innovation, and Digitalization through the National Research, Development, and Innovation Plan 2022–2027, Core Program, project number PN 23 05, contract number PN11N-03-01-2023.

## CREDIT AUTHORSHIP CONTRIBUTION

GIDEON GWANZUWANG DANKAT: writing (original draft preparation), methodology, validation.
GEORGE CRISTIAN LAZAROIU: funding acquisition, review, supervision.
LAURENTIU MARIUS DUMITRAN: conceptualization, review, supervision, formal analysis.
ANCA CONSTANTINA PARAU: resources, hardware.
ALINA VLADESCU (DRAGOMIR): resources, hardware.

*Received on 5 March 2026*

## REFERENCES

1. M.Y. Shtern, B.R. Mustafoev, E.P. Korchagin, A.O. Kozlov, M.S. Rogachev, *Investigation of contact resistance in the structure of thermoelements*, 2021 IEEE Conference of Russian Young Researchers in Electrical and Electronic Engineering (ElConRus), St. Petersburg, Moscow, Russia, pp. 2476–2480 (2021).
2. W. Ta et al., *Volumetric contact theory to electrical contact between random rough surfaces*, Tribology International, **160**, pp. 1–10 (2021).
3. ***Grand View Research, *Automotive connectors market*, pp. 1–10 (2026).
4. ***Verified Market Research, *Automotive connector market*, pp. 1–10 (2026).
5. S. B. et al., *Performance investigation of single-phase transformerless PV inverter connected to low voltage network*, Rev. Roum. Sci. Techn. – Électrotechn. et Énerg., **69**, *1*, pp. 55–60 (2024).
6. J. Swingler, J.W. McBride, *The degradation of road-tested automotive connectors*, Electrical Contacts – 1999. Proceedings of the Forty-Fifth IEEE Holm Conference on Electrical Contacts, pp. 146–152 (1999).
7. W. Shujuan, H. Fang, S. Bonan, Z. Guofu, *Method for calculation of contact resistance and finite element simulation of contact temperature rise based on rough surface contact model*, 26th International Conference on Electrical Contacts (ICEC 2012), pp. 317–321 (2012).
8. Y. Shibata et al., *Detailed analysis of contact resistance of fretting corrosion track for the tin-plated contacts*, 26th International Conference on Electrical Contacts (ICEC 2012), pp. 228–232 (2012).
9. Y. Fukuyama, N. Sakamoto, N.-H. Kaneko, T. Kondo, M. Onuma, *Constriction resistance of physical simulated electrical contacts with nanofabrication*, 2014 IEEE 60th Holm Conference on Electrical Contacts (Holm), pp. 1–5 (2014).
10. C. Weißenfels, P. Wriggers, *Numerical modeling of electrical contacts*, Computational Mechanics, **46**, pp. 301–314 (2010).
11. R.S. Timsit, *Electrical conduction through small contact spots*, Proceedings of the 50th IEEE Holm Conference on Electrical Contacts and the 22nd International Conference on Electrical Contacts, pp. 184–191 (2004).
12. Y. Fukuyama, N. Sakamoto, T. Kondo, J. Toyoizumi, T. Yudate, N.H. Kaneko, *Experimental measurements of constriction resistance for electrical contacts simulated using microfabrication*, IEEE Transactions on Components, Packaging, and Manufacturing Technology, **8**, *6*, pp. 927–931 (2018).
13. J. Lim, H. Kim, J.K. Kim, S.J. Park, T.H. Lee, S.W. Yoon, *Numerical and experimental analysis of potential causes degrading contact resistances and forces of sensor connectors for vehicles*, IEEE Access, **7**, pp. 126530–126538 (2019).
14. A. Ethirajan, R. Ramabadran, *Power loss analysis and control of a bidirectional high-gain converter for EV charging using PV array*, Rev. Roum. Sci. Techn. – Électrotechn. et Énerg., **71**, *1*, pp. 33–38 (2026).
15. G.G. Dankat, L.M. Dumitran, A.V. Dragomir, A.C. Parau, *Influence of accelerated aging on the electrical resistance of copper contacts with ZrCu discontinuous thin layer*, 2023 13th International Symposium on Advanced Topics in Electrical Engineering (ATEE), Bucharest, Romania, pp. 1–6 (2023).
16. G.G. Dankat, L.M. Dumitran, A.V. Dragomir, A.C. Parau, *Numerical and experimental study of aging on electrical resistance of copper connectors with ZrCu discontinuous thin layer*, 2025 14th International Symposium on Advanced Topics in Electrical Engineering (ATEE), Bucharest, Romania, pp. 1–6 (2025).
17. M. Braic et al., *A comparative study of the structural, mechanical and tribological characteristics of TiSiC-Cr coatings prepared in $CH_4$ and $C_2H_2$ reactive atmosphere by cathodic vacuum arc*, Applied Surface Science, **400**, pp. 318–328 (2017).
18. A. Brognara, J.P. Best, P. Djemia, D. Faurie, G. Dehm, M. Ghidelli, *Effect of composition and nanostructure on the mechanical properties and thermal stability of $Zr_{100-x}Cu_x$ thin film metallic glasses*, Materials & Design, **219**, pp. 1–10 (2022).
19. J.P. Chu, J.S.C. Jang, J.C. Huang, H.S. Chou, Y. Yang, J.C. Ye, Y.C. Wang, J.W. Lee, F.X. Liu, P.K. Liaw, Y.C. Chen, C.M. Lee, C.L. Li, C. Rullyani, *Thin film metallic glasses: Unique properties and potential applications*, Thin Solid Films, **520**, *16*, pp. 5097–5122 (2012).
20. M. Braic, V. Braic, A. Vladescu, C.N. Zoita, M. Balaceanu, *Solid solution or amorphous phase formation in TiZr-based ternary to quinternary multi-principal-element films*, Progress in Natural Science: Materials International, **24**, *4*, pp. 1–10 (2014).
21. J. Song, H. Schmidt, *Electrical resistance of connectors with different contact finishes under low-level conditions*, Proceedings of the 55th IEEE Holm Conference on Electrical Contacts, Vancouver, BC, Canada, pp. 334–338 (2009).
22. Y. Fukuyama et al., *The effect of the distribution of a-spots in the peripheral part of an apparent contact point on the constriction resistance*, Proceedings of the 2017 IEEE Holm Conference on Electrical Contacts, Denver, CO, USA, pp. 302–305 (2017).
23. H. Tanimoto, K. Takeuchi, T. Ikegami, T. Okazaki, *Inhibition of electropulsing nanocrystallization in amorphous ZrCu under helium atmosphere*, Materials Transactions, **61**, *5*, pp. 878–883 (2020).